The Physics Document

CosmicWatch
The Desktop Muon Detector (v3X)

Contacts:
Prof. Spencer N. Axani (saxani@udel.edu)
Masooma Sarfraz (masoomas@udel.edu)
Miles Garcia (milesg@udel.edu)
Katarzyna Frankiewicz (katarzyna.frankiewicz@gmail.com)
Prof. Janet M. Conrad (conradg@mit.edu)

August 20, 2025

Contents

Chapter 1

Document Overview

The CosmicWatch Detector v3X is a compact, self-contained, inexpensive (100$), low-power (0.5 W), particle detector that uses a plastic scintillator and silicon photomultiplier to explore particle, nuclear, astro-, and geophysics. Through these detectors we can explore a wide range of phenomena, including muon energy loss in materials, special relativity, radioactive decay, cosmic ray shower composition, and much more. The detectors support standalone data logging to microSD or live USB streaming, offers coincidence mode for background suppression, and logs rich event metadata (e.g. timestamp, ADC value, temperature, pressure, acceleration, and angular velocity). The detector is free to use, share, and adapt only in non-commercial contexts. It will be useful for education, outreach, citizen science, and more advanced physics studies.

The Physics Document discusses the physics associated with measurements performed in the Example Measurements Document for the Desktop Muon Detectors v3X. It starts by describing the sources of ionizing radiation that we need to consider for the remainder of the document. After that, we'll work through how each of these forms of radiation interact with materials and how the detectors measure their interaction. We'll then shifts to details specific to the detectors, discussing the technology employed. If you would like to build a detector, simply follow the instruction found in the Instruction Manual.

All material for v3X can be found in the GitHub repository located here:

`https://github.com/spenceraxani/CosmicWatch-Desktop-Muon-Detector-v3X`

Many documents have played a crucial role in compiling this information. A great and valuable reference, is the Particle Data Group's (PDG) summary on cosmic rays [1] and energy loss in matter [2]. MIT Prof. Bruno Rossi's textbook, *Cosmic Rays* from 1964 [3], is a great entry-level resource, providing an early account of cosmic-ray physics investigations. It not only offers

insightful reading but also allows readers to replicate many of the experiments conducted for the first time using the CosmicWatch detectors.

For a more contemporary perspective with a focus on history, Prof. M. Friedlander's book titled *A Thin Cosmic Rain* [4] is recommended. Dr. P. Grieder's comprehensive textbook, *Cosmic Rays at Earth* [5], provides an in-depth overview of cosmic-ray physics and will be frequently referenced. For higher-energy cosmic-ray physics, Prof. T. Gaisser's book (from the University of Delaware), *Cosmic Rays and Particle Physics* [6], proves to be extremely useful.

For a comprehensive understanding of energy loss in matter, *Techniques for Nuclear and Particle Physics* by W. Leo [7] stands out as one of the best resource for experimental particle physics. Additionally, Prof. C. Grupen's textbook, *Particle Detectors* [8] and *Particle Detectors: Fundamentals and Applications* [9] by H. Kolanoski, are extremely highly recommended as a reference for describing detection methods in particle physics.

Chapter 2

Sources of ionizing radiation

Our discussion commences with an exploration of the diverse sources of ionizing radiation that can activate the Desktop Muon Detectors. Some forms of ionizing radiation hold particular significance due to their prevalence and energy levels. Additionally, we will touch upon why certain other forms of ionizing radiation do not register on our sensitivity, though a brief description of them is included for comprehensive understanding.

2.1 Cosmic radiation

The Earth is continuous bombarded by particles known as *cosmic rays*. About 74% (by mass) of this cosmic-ray flux originates from ionized hydrogen (free protons), 18% from helium nuclei (two protons and two neutrons), and the remaining portion consists of trace amounts of heavier elements [1]. A significant fraction of the observed cosmic-ray flux at Earth is relativistic, meaning that the individual nuclei possess kinetic energies greater than their rest mass ($\mathrm{E}_k/\mathrm{m}c^2 > 1$).

Lower energy cosmic-rays (GeV-scale) are significantly influenced by the solar wind and the Earth's geomagnetic field, as depicted in Fig. 2.1. These factors limit the flux interacting with the Earth. The high-energy flux extends up to 10^{11} GeV, beyond which cosmic rays lose energy through interactions with the cosmic microwave background, known as the GZK cutoff[1].

The energy of cosmic rays decreases rapidly: below 10^6 GeV, the flux decreases as $\mathrm{E}^{-2.7}$, and above this, it steepens to approximately $\mathrm{E}^{-3.1}$ [6]. To provide perspective, the number of 1 GeV cosmic-ray protons is 8.1 orders of magnitude higher than that at 1000 GeV (i.e., 2.7×3), or

[1]The highest energy cosmic-ray observed, approximately 3×10^{20} eV [10] (48 joules), equivalent to a brick falling on your toe [11], was contained in a single proton and later named the *Oh-My-God Particle*.

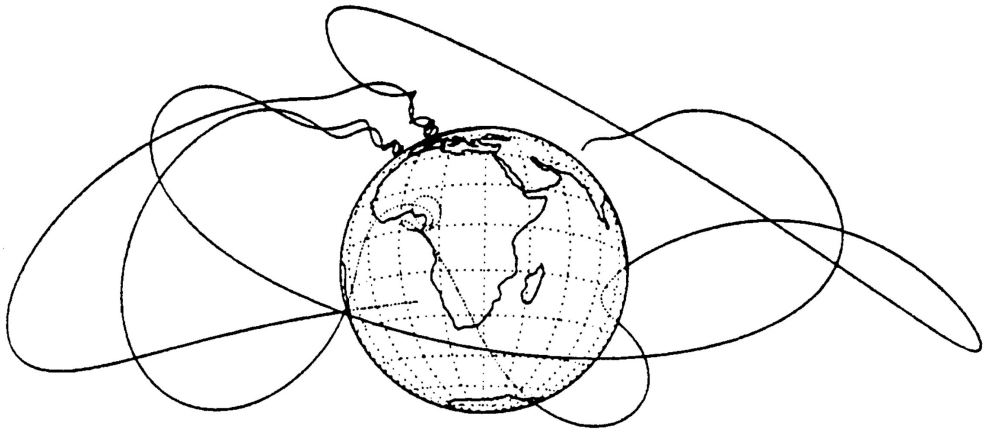

Figure 2.1: Simulated trajectories of low energy cosmic-rays interacting with the geomagnetic field. From Ref. [4]

16.2 orders of magnitude higher[2] than that at 10^6 GeV (i.e., 2.7×6).

When a primary cosmic-ray collides with a nucleus in the upper atmosphere (typically an oxygen or nitrogen nucleus), the energies involved can break apart either the primary particle or the target nucleus through nuclear interactions. The collision energy produces short-lived particles called *mesons*[3]. The most common mesons are the π-meson or pion (π^+,π^-,π^0) and the K-meson or kaon (K^+,K^-,K^0). Charged pions ($\pi\pm$) decay within approximately ten billionths of a second, producing muons and neutrinos (charged kaons, $K\pm$, are more complex in their decay, but they also preferentially decay this way or to pions). Neutral mesons (π^0, K^0) decay about one billion times faster (10^{-17}s) than charged mesons, primarily to gamma rays. Unlike neutral mesons, charged mesons can travel sufficiently before decaying to interact with another molecule in the atmosphere. This interaction may result in another nuclear interaction, similar to the primary cosmic-ray interaction, generating more mesons and contributing to the particle shower induced by the primary interaction.

Primary cosmic rays do not directly penetrate Earth's surface due to atmospheric shielding. However, a small flux of nuclear fragments (such as protons and neutrons) from these interactions can occasionally cascade down and reach the surface. Figure 2.2 illustrates a cosmic-ray interaction, with the initial interaction of vertical cosmic rays occurring at an altitude approximately between 15 and 20 km. Cosmic rays entering at an angle will interact at higher altitudes due to their path traversing more atmosphere [14].

The high energy photon from the decay of the neutral mesons quickly materialize into an

[2]The steep decrease in energy of the cosmic-ray flux necessitates large detectors for measuring rare high-energy events.

[3]Mesons, unlike protons and neutrons, contain only two quarks: one quark and one anti-quark. The lightest meson is the pion, followed by the kaon. Although there are many other quark/anti-quark pair combinations, their higher masses make them less preferentially produced and are not discussed here [12, 13].

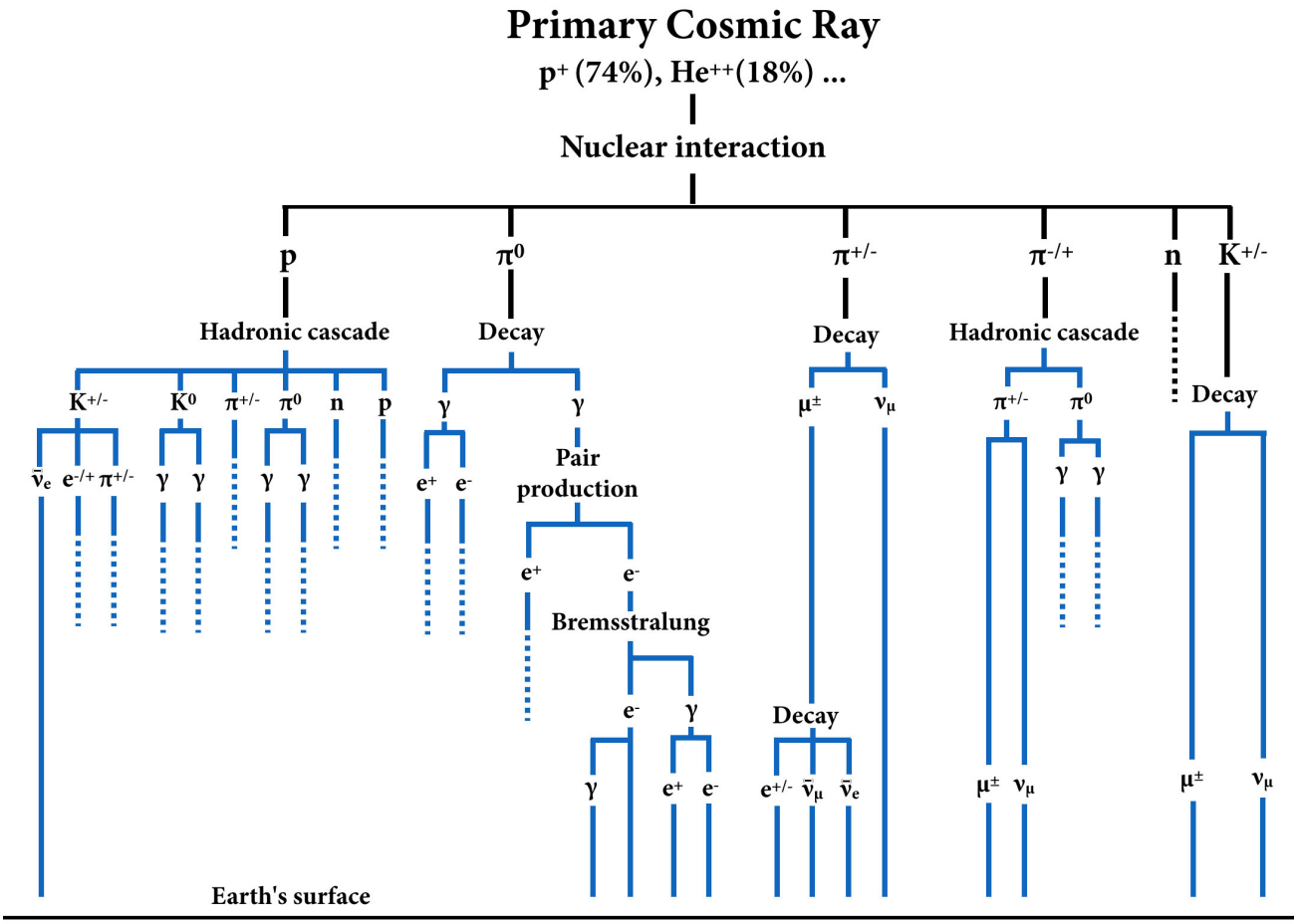

Figure 2.2: An schematic representation of the various decay and interactions chains that result from the interaction of a cosmic-ray in Earth's atmosphere. This is a modified figure from Ref. [3].

electron-positron pair, also referred to as *pair production*. These electron-positron pairs then radiate high energy photons, which can again materialize into another electron-positron pair. This electromagnetic cascade process continues, dividing the original energy of the photons between the numerous electrons, positrons, and lower energy photons at the end of the cascade. Photons with energies less than 1.022 MeV cannot further pair produce and their interactions will be dominated by Compton scattering and photoelectric absorption. At lower altitudes, there isn't a fresh supply of high energy neutral mesons due to the rapid decrease of nuclear interactions at lower altitudes.

The cosmic-ray muons ($\mu^{\pm}$) originate from the decay of the charged mesons. A charged pion will decay to a same-sign muon (and muon-neutrino) with a branching fraction of 99.98%, whereas a charged kaon decays to a muon (and muon-neutrino) 63.5% of the time [15]. The neutrinos are not electrically charged and only interact through the weak force, therefore they can be fully ignored in this discussion.

$$\begin{aligned} \pi^{\pm} &\rightarrow \mu^{\pm} + \nu_{\mu}(\bar{\nu}_{\mu}) \text{ ... } (99.98\%) \\ K^{\pm} &\rightarrow \mu^{\pm} + \nu_{\mu}(\bar{\nu}_{\mu}) \text{ ... } (63.5\%) \end{aligned} \tag{2.1}$$

Approximately 80-90% of the muon flux in the energy range of interest (GeV to TeV-scale) comes from the decay of pions, and the remainder from kaons [16]. The muons are particularly penetrating, that is, they essentially only lose energy due to ionization as they travel through the atmosphere and other matter and can make it through a large amount of material. This is contrasted with *baryons* (particle comprised of quarks), which also interact through the strong force. This makes muons the most numerous charged particle showering down on the Earth's surface. Muons have a mass of 105.65 MeV and are also unstable particles with a half-life of 2.2 $\times 10^{-6}$s. They decay to an electron and two neutrinos:

$$\mu^{\pm} \rightarrow e^{\pm} + \nu_e(\bar{\nu}_e) + \bar{\nu_{\mu}}(\nu_{\mu}) \text{ ... } (100.0\%), \tag{2.2}$$

however, again we can ignore the neutrinos. A cosmic-ray muon with an energy greater than 2.4 GeV will be sufficiently relativistic that its half-life, as seen by an observer on the Earth, will be dilated enough that it has a significant chance of reaching the Earth's surface before decaying. In other words, the muon decay length becomes greater than 15 km – the approximate altitude of the cosmic-ray muon production. Further, a typical muon will lose approximately 2 GeV of energy due to ionization as it passes through the atmosphere on its way to the ground. Combining these two facts with the fact that the geomagnetic field and interstellar solar winds drive back the GeV-scale cosmic-rays, as well as the steeply falling cosmic-ray energy spectrum, we can expect the average muon energy at Earth's surface to be greater than a few GeV. We typically quote the mean cosmic-ray muon energy at Earth's surface to be approximately 4 GeV [1]. The muons that do not survive the journey to the Earth's surface decay. The resulting electrons (or positrons in the case of a μ^+), also referred to as *Michelle electrons*, contribute to the low energy electromagnetic component from cosmic-ray showers at sea level.

At sea level, the angular distribution of cosmic-ray muons can be well approximated by a $\cos^2\theta$ dependence, where θ is the zenith angle–the angle between the direction of the incoming muon and the vertical. This angular dependence arises from the increased path length through the atmosphere that muons must traverse at larger zenith angles. A muon incident vertically travels through roughly 15-20 km of atmosphere, whereas one arriving from the horizon traverses over 400-500 km. The increased path length leads to a higher probability of decay and greater energy loss due to ionization before reaching the detector. As a result, fewer muons arrive from near-horizontal directions. The $\cos^2\theta$ dependence thus reflects both geometric projection effects and the attenuation of muons due to their finite lifetime and energy loss.

Let us now compare the number of particles showering down on us at sea level. We'll limit ourselves to thinking about particles that are coming from one steradian about the zenith, this can be thought of as circular disk around the vertical (zenith) part of the sky whose area represents approximately $1/6^{th}$ of the total visible sky, or equivalently, a half-angle of 32° from the zenith. From this direction, we can describe the number of particles passing through a

1×1 cm^2 horizontal surface per minute (cm^{-2} min^{-1} sr^{-1}) by following the measurements outlined in Ref. [1]. We expect approximately 0.4 cm^{-2} min^{-1}sr^{-1} from $\mu^{\pm}$ with energies greater than 1 GeV; 0.2 e$^{\pm}$ cm^{-2} min^{-1}sr^{-1} above 10 MeV, but the flux falls off fast with energy, becoming negligible above 1 GeV; and 0.0054 cm^{-2} min^{-1}sr^{-}1 from protons above 1 GeV; and a charged meson flux above 1 GeV two orders of magnitude lower than that of the proton flux. This means that the protons and charged mesons are insignificant at sea level, however, there is a significant muonic and low-energy electromagnetic component. In Ref. [5], the flux is divided into a hard component (essentially fully muons), which can penetrate 15 cm of lead, and soft component (approximately 60-65% muons and the remainder is electrons, positrons, and photons), which cannot. As we'll soon see, there are a variety of physical phenomena that influence fluxes, but the relative contributions listed here represent a useful approximation.

As we increase in altitude, the relative contribution from the ionizing radiation fluxes change. In particular, we see a larger contribution from both the protons and electromagnetic component, whereas the charged mesons are still sub-dominant. Once we pass the primary interaction region where the primary cosmic-rays are most likely to interact (typically around 15-20 km), the secondary particles produced by the initial nuclear interaction die off and we see a decrease in the ionization radiation flux. The shape of the curve describing the ionizing radiation flux as a function of altitude is called the Pfotzer curve, and where the ionizing particle production reaches a maximum is termed the Regener-Pfotzer maximum [17].

2.1.1 Flux variations due to solar system properties

There are several properties associated with the interstellar medium that modulate the cosmic-ray flux, and in particular the observable cosmic-ray muon flux. These properties are primarily associated with behaviour of the Earth and Sun's magnetic field.

The latitude effect: Roughly speaking, the Earth has a magnetic field that behaves similarly to a magnetic dipole orientated from north to south. The magnetic field points parallel to the surface of the Earth near the equator, and perpendicular to the surface near the poles. Particles traveling towards the Earth will be less deflected (F=q$\vec{v} \times \vec{B}$) near the poles compared to the equator. Low energy charged particles passing through the magnetic field may even become trapped in what's known as the *Van Allen radiation belt*. This presents a low energy cutoff, where the magnetic field is able to deflect protons below approximately 10 GeV near the equator (corresponding to a rigidity of 10 GV) and near 1 GeV at higher latitudes [18, 19].

The East-West asymmetry: The cosmic-ray muon flux is larger looking towards the west compared to the east due to the Earth's magnetic field. This is an effect produced by primary cosmic-ray particles being predominately positively charged. The positively charged muons curve towards the east, meaning that the intensity from the west is stronger. This effect is more evident in the upper atmosphere [5], and obviously a larger effect at the geomagnetic equator than at the poles.

Magnetic anomalies: There are local geomagnetic field variations, which causes a change in the cosmic-ray intensity. The most prominent being the *South Atlantic Anomaly (SAA)* [20], which extends from the east coast Brazil to the west coast of southern Africa (-50.0 to 0.0 geographic latitude and from -90.0 to 40.0 longitude). This is the region where Earth's inner Van Allen radiation belt extends closest to the planet's surface and provides the smallest amount of protection from cosmic-rays. In fact, the increased level of ionizing radiation when passing through the SAA is responsible for radiation damage to electronics on-board Low-Earth Orbit (LEO) satellites[4].

Solar modulation: The observed cosmic-ray flux at the top of the Earth's atmosphere depends partially on solar activity, which manifests itself as an 11-year cycle[5]. Solar winds can drive back low energy cosmic-rays entering the solar sphere and the modulation effect decreases with an increase in energy. According to Ref. [14], the 1 GeV cosmic-ray proton flux is twice as small during maximum solar activity compared to minimum solar activity; similarly there is a 10% reduction in the 10 GeV cosmic-ray protons during the solar maximum.

Solar Flares: Solar-flares can eject protons with energies up to several GeV, the upper end of which is able to produce muons through nuclear interactions. These events are rare transients, and since the energy is low, it primarily has an effect on the low energy muon flux [26].

2.1.2 Flux variations due to atmospheric properties

Similar to the previous subsection, there exists terrestrial phenomena that also modulate the cosmic-ray muon flux.

The Cosine Squared Law: At greater angles from the vertical, cosmic-ray muons must travel through a much larger distance, and therefore amount of matter, to reach a ground-based observer. A cosmic-ray muon traveling vertically downwards may only travel through 15 km of atmosphere, whereas one traveling in the horizontal direction must pass through approximately 500 km of atmosphere. The larger path length means that the muon will lose more total energy due to ionization in the atmosphere and also have a higher probability of decaying before reaching the ground. As a function of zenith angle, the cosmic-ray muon intensity is expected to follow a cosine squared dependence [1].

The atmospheric attenuation: Recall that the nuclear interactions between the primary cosmic-ray and atmospheric nucleus happen in the upper atmosphere. Therefore, particles

[4]The International Space Station (ISS) passes intermittently through the SAA [21] and has dedicated instrumentation for measuring the increased radiation dose to astronauts [22]. Astronauts from NASA missions as early as Apollo 11 [23] have also reported seeing flashes of light while being in orbit [24]. These flashes of light are attributed to high-energy particles in the space radiation environment, however many details on the origin are still unknown [25]

[5]There is also a 22-year cycle since the solar magnetic dipole flips polarity at every solar maximum, which occurs every 22 years [5]

reaching sea level must have had sufficient energy to penetrate the remainder of the atmosphere. An increase in atmospheric density (perhaps due to atmospheric pressure changes) will cause secondary particles to lose more energy as they propagate to the Earth's surface. Due to this, the muon rate turns out to be anti-correlated with the pressure (i.e. if the atmospheric pressure increases, the cosmic-ray muon rate decreases). The density of the atmosphere changes with the season and therefore exhibits a time-dependence. From other measurements, this is expected to be a percent level effect [27].

The positive temperature effect: To produce a muon, we require a charged meson to decay. However, recall that the charged mesons are typically relativistic and have lifetimes on the order of nanoseconds[6]. This gives the charged mesons sufficient time to potentially interact with another nucleus in the atmosphere rather than decay. As the temperature increases, the atmosphere expands and there are fewer particles to interact with, thus increasing the probability of decaying rather than interacting [28].

Rather than correlating this with the ground based pressure (as in the paragraph above), it is more commonly correlated with atmospheric temperature – taking into account the temperature profile of the atmosphere. This effect is larger at higher energies and therefore is typically measured in laboratories located deep underground where the low energy cosmic-rays have less of an influence [29–31].

The negative temperature effect: As the temperature of the atmosphere increases, the atmosphere expands, moving the muon production region further out. This means that the muon path length increases, which gives them a higher probability of decay prior to making it to the ground. During the winter when the atmosphere is colder, shallower and more dense, cosmic-ray interactions happen closer to the Earth's surface. The charged mesons quickly begin to lose energy and have a less likely chance of decaying into muons.

2.2 Radioactive backgrounds

The previous section described the ionizing radiation that we expect from showers of particles raining down from the upper atmosphere, and the expected phenomena that can modulate this flux. This section will describe ionizing radiation that originates on the surface of Earth and can also influence our measurements; we'll refer to these as the *radioactive backgrounds*. Radioactive backgrounds are sub-divided into primarily three main processes called alpha, beta, and gamma radiation. Radioactivity is a quantum mechanical effect, which is non-deterministic, that is, we cannot predict when a particle will decay, rather we can only assign a probability to it. The energy scale of these processes are relatively low (MeV-scale) compared to the energies

[6]For example, a 5-GeV $\pi^{\pm}$ produced at 15 km will travel approximately 300 m before decaying. This distance is small compared to the interaction path length of approximately 13 km, which means that most charged pions will decay rather than interact. However, at approximately 115 GeV, the pion has an equal probability to interact or decay in the atmosphere.

associated with the cosmic-rays (GeV and above), but their natural abundance on the surface of the Earth is sufficient that these are typically the dominant source of triggers in the Desktop Muon Detector.

Alpha decay is the result of an unstable nucleus ejecting a helium nucleus (a bound state of two protons and two neutrons), $(Z, A) \rightarrow (Z-2, A-4) + \alpha$. This is a quantum mechanical effect, where a helium state (helium is a very tightly bound state) forms in the nucleus, then quantum tunnels through the nuclear potential barrier, exiting the nucleus. The emitted alpha particle is mono-energetic, and since the helium nucleus has a charge of +2e and mass of approximately 4 GeV (therefore, it moves slow and has a large charge), it will lose energy rapidly in matter. A 5-MeV alpha particle will have a range of 3.5 cm in air before losing all of its energy, or equivalently, 23 micrometers in aluminum[7] [32].

Beta radiation is described as the decay of a neutron to a proton[8]: $n \rightarrow p + e^- + \bar{\nu}_e$. The proton remains in the nucleus, while the electron and electron-neutrino are ejected. Since this is a 3-body decay, the electron is not mono-energetic. It is emitted with a continuous energy spectrum whose maximum energy is approximately at the total energy available for the decay (the Q-value). Beta decays typically have energies that can range from tens of keV to a few MeV.

Gamma radiation is simply a high-energy photon, emitted during the de-excitation of an atomic nucleus. When the nucleus is in an unstable state (for example, maybe the nucleus absorbed a neutron or was left in an excited state after a beta decay), it will de-excite into a lower energy configuration releasing a photon. This is analogous to the de-excitation of an atomic electron, emitting a characteristic mono-energetic photon. Since the energy levels in the nucleus are quantized, gamma ray are also mono-energetic (with a small spread due to nuclear motion). These energy scales are in the 100 keV to MeV-range.

[7]The high energy loss rate that alpha radiation makes it useful for cancer therapies. An alpha particle will deposit all of its kinetic energy into a very local space (order micrometers in human tissue), which is capable of destroying cancerous cells.

[8]More fundamentally, during neutron decays, a down-quark in the neutron converts to a up-quark, emitting a virtual W-Boson $u \rightarrow d + W \rightarrow d + e^- + \bar{\nu}_e$. On the macroscopic level, this appears as the transmutation of an atom converting to another atom with an extra proton and one fewer neutron: $A(Z, N) \rightarrow A'(Z+1, N-1) + e^- + \bar{\nu}_e$.

Chapter 3

Particle interactions with matter

To identify a particle, it is essential for it to engage in an interaction with the detector's material, facilitating the transfer of energy from the particle to the absorbing substance. This segment will delve into the primary interactions that effectively transmit energy from particles like muons, protons, pions/kaons, and other high-energy heavy charged particles. Subsequently, we will explore interactions related to high-energy electrons (including positrons) and conclude with those associated with radioactive backgrounds.

3.1 High energy heavy charged particles

The following explanation proves valuable when considering any charged particles with a mass significantly greater than that of the electron ($m \gg m_e$). This encompasses all charged particles except for the electron and positron. For instance, the muon, the next lightest charged particle, is 206 times more massive than the electron. In contrast to the linear trajectories of heavy charged particles, electrons do not follow straight paths within a target, necessitating special consideration. The description provided below offers an approximation of the fundamental processes contributing to energy loss in matter, acknowledging that the scope of this topic is too extensive to cover comprehensively in a single document. More information can be found in Ref. [2, 8, 33, 34].

The rate of energy loss, often denoted as stopping power (-dE/dx), quantifies the amount of energy lost per unit distance traveled. It is commonly measured in units of MeV cm^2/g, known as *mass stopping power*. To obtain the energy lost per centimeter, one simply multiplies this value by the density (in g/cm^3) of the material being traversed. To facilitate comparisons, we express the energy loss rate in terms of water ($\rho = 1.0\ g/cm^3$), which conveniently shares a similar density with plastic scintillator. As a particle moves through a substance, its energy loss can be categorized into three mass-dependent ranges:

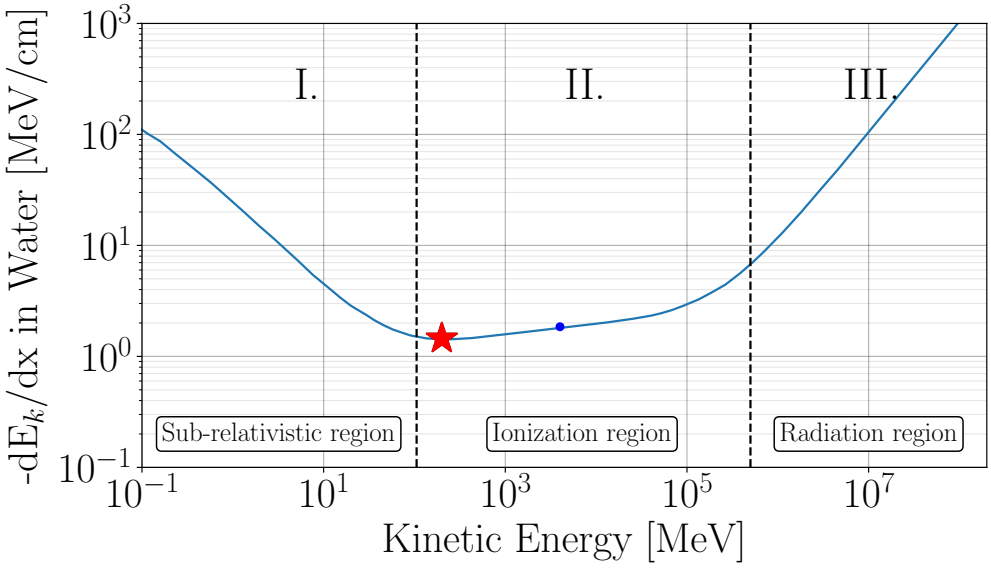

Figure 3.1: The kinetic energy loss per centimeter traveled, of a muon traveling through H_2O ($\rho = 1.0 g/cm^3$). Modified from Ref. [35]. The blue dot represents the mean energy of the cosmic-ray muons at sea level (4 GeV), and the red star represents where the particle is minimally ionizing.

- I. The sub-relativistic region: ($E_k < mc^2$)
- II. The ionization region: ($E_k > mc^2$ and $E < 400$ GeV m^2/m_μ^2)
- III. The radiation region ($E > 400$ GeV m^2/m_μ^2).

The delineation of these three regions is depicted in Fig.3.1 for a muon traversing water. However, the energy loss can be adapted to another material by straightforwardly multiplying it by the density (in g/cm^3) of that material. For instance, the stopping power in lead would be adjusted by a factor of 11.34. Similarly, the energy loss can be tailored to a different particle by multiplying it by the square of the particle's charge. For instance, the energy loss of an alpha particle would be scaled by a factor of 4. While this plot is commonly presented in terms of momentum, we have scaled it using the kinetic energy of the incident particle for simplicity in explanation. The vertical dashed lines, marking the boundaries of the three regions, can be adapted to another charged particle using the aforementioned principles. For instance, a proton would enter the sub-relativistic region at approximately 1GeV.

In the **sub-relativistic region** (Muon: $E_k \approx 100$ MeV; Proton: $E_k \approx 1$ GeV), As the particle loses energy, the rate of energy loss per unit distance traveled increases. Essentially, this implies that once a particle enters this region, it rapidly decelerates and comes to a stop quickly. This phenomena is also known as the *Bragg peak* [7].

In the **high energy radiation region** (Muon: $E_k \approx 400$ GeV; Proton: $E_k \approx 27$ TeV), the

energy loss is associated with *bremsstrahlung*, pair production, and nuclear interactions, and scales linearly with energy. The radiation term becomes predominant at around 400 GeV for muons. However, it's important to note that the cosmic-ray flux decreases rapidly with energy. Muons in this energy regime constitute only a small percentage of the overall flux and experience rapid energy loss.

Finally, the **ionization region** encompasses the majority of the cosmic-ray muon flux. It is noteworthy that the mean muon energy at sea level is 4GeV, as indicated by a blue marker in Fig.3.1. The energy loss in this region results from ionization (breaking electromagnetic bonds) and excitation (raising the electron to a higher-lying shell within the absorber atom) of the incident particle. This behavior is described by the *Bethe Bloch formula*. Detailed explanations of the formula can be found in Refs. [7, 8, 35]).

This region is particularly fascinating because the energy loss rate remains nearly constant (increasing logarithmically), with an average energy loss rate of 2.,MeV/cm in a material with a density of $1.0\,\mathrm{g/cm^3}$ across many orders of magnitude. The minimum point, denoted by a red star in Fig.3.1, designates the muon as a minimum ionizing particle (MIP), representing the energy at which the muon is most penetrating. The function exhibits such a flat trend in the vicinity of this minimum (up to approximately 400 GeV) that any particle with energy near this red star is commonly referred to as a MIP. Interestingly, the majority of the cosmic-ray flux falls within this region. Consequently, to estimate the penetrating depth of a typical cosmic-ray muon, one can simply divide the energy by $2.2\,\mathrm{MeV/cm}$ and multiply by the density of the absorber. For instance, a 10GeV muon can penetrate through approximately 17m of concrete (ρ= $2.7\,\mathrm{g/cm^3}$).

As for other heavy charged particles discussed in this document—protons, pions, and kaons—they also lose energy through ionization. However, due to their composition of quarks, they can also interact via the strong force. The strong force is responsible for nuclear collisions that can significantly impact the particle and its trajectory. This unique property makes muons stand out—they do not interact via the strong nuclear force, and being heavy allows them to penetrate through materials with minimal losses due to collisions with electrons in the absorbers and with minimal deflection in their trajectory[1].

3.2 High energy electrons/positrons and photons

As discussed in Section 2.1, a notable source of electrons/positrons with energies below 1 GeV showers onto the Earth's surface. This section focuses on describing the energy loss for high-

[1]Given their ability to penetrate very large distances through materials, many experiments are situated kilometers underground to shield against high-energy muons. For example, the neutrino detector Super-Kamiokande is buried underneath a 1-km mountain in Japan to reduce the muon flux by a factor of 10^5, preventing them from overwhelming the search for rare, less energetic interactions from neutrinos. Similarly, the IceCube neutrino detector is buried under 1.4 km of ice in the Antarctic glacier at the South Pole for similar reasons.

energy electrons, with the understanding that the explanation is equally applicable to positrons. For electrons above a few tens of MeV, radiation losses, primarily through *bremsstrahlung radiation* (translated as "braking radiation" in German), dominate the energy loss mechanism. Bremsstrahlung radiation involves the emission of photons when a particle accelerates and decelerates in the vicinity of the electric field of the material's nucleus.

A bremsstrahlung photon with sufficient energy can undergo pair production, yielding an electron and positron, which subsequently emit additional bremsstrahlung photons, initiating a cascade of electrons, positrons, and photons. This process governs the energy loss of the electron until its energy drops below a few tens of MeV, commonly referred to as the critical energy. Remarkably, the radiation energy loss rate scales with energy. In the region above the critical energy, the rate of energy loss (dE/dx) is proportional to the energy. Consequently, a 20GeV electron, for instance, initially loses energy per centimeter traveled at a rate 1000 times greater than a 20MeV electron, predominantly through bremsstrahlung radiation. This leads to a rapid decrease in the energy of high-energy particles as a function of distance traveled.

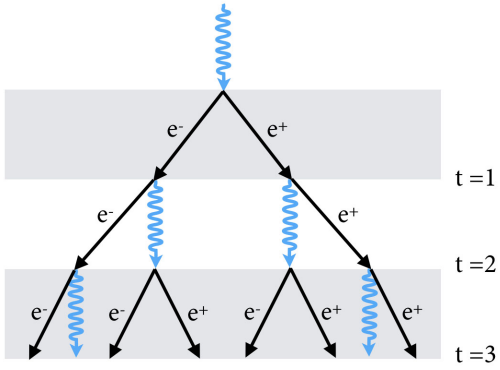

Figure 3.2: The Heitler Model for electromagnetic cascades.

A *radiation length*, denoted as X_0, is defined as the average thickness of a material that reduces the mean energy of an electron or positron by a factor of $1/e$ (Euler's number $= 2.71828$) due to bremsstrahlung radiation. In practical terms, this implies that an electron will lose a factor of e^{-t} energy after traversing t radiation lengths. For instance, after four radiation lengths, a 1 GeV electron will end up with approximately 20 MeV. The simplified *Heitler Model for electromagnetic cascades* approximates this by stating that one electron-positron pair will be created per radiation length, and each pair will receive half of the energy of the photon that produced them. After t radiation lengths, the cascade will contain 2^t particles (electrons, positrons, and photons), each with an average energy of approximately $E = \frac{E_0}{2^t}$ [36]. This concept is illustrated in Fig. 3.2.

A valuable list of radiation lengths for various materials is provided in Table 3.1. This table includes information about materials relevant to the Desktop Muon Detectors or used in some measurements below.

3.3 Low energy electrons/positrons

Electrons and positrons, being the lightest charged particles, exhibit qualitative behavior in electron scattering distinct from that of high-energy particles in two ways. Firstly, the energy

Material	Density [g/cm^3]	Radiation length [cm]	Critical Energy [MeV]
Water (H_2O)	1.00	36.1	92
Lead (Pb)	11.35	0.56	9.51
Concrete	2.5	10.7	
Air at STP*	1.2931	30420	102
Scintillator (Polystyrene)	1.032	42.4	109
Aluminium (Al)	2.70	8.9	51.0

Table 3.1: A table of materials that are mentioned in this document and their corresponding radiation length. *STP indicates that the air is at the standard temperature and pressure: 20°C and 101.325 kPa. The data was collected from Ref. [1, 7].

loss by electrons fluctuates significantly more than that of heavy particles. For instance, the maximum transferable kinetic energy of a 4 GeV electron is the full 4 GeV (given their equal masses), whereas a muon with the same energy has a maximum transferable energy of approximately 1 GeV. Secondly, due to their small mass, electrons are particularly prone to experiencing large-angle deflections when scattering off a nucleus. This susceptibility is so pronounced that multiply scattered electrons may undergo a complete reversal in direction, a phenomenon defined as *backscattering*. The probability of backscattering is higher at lower energies, and if backscattered, electrons do not deposit all their energy in the absorbing medium. For instance, a 1 MeV electron has approximately a 10% chance of backscattering off a thick slab of aluminum, and a 50% chance of backscattering off a slab of gold. [37].

The previous section described electrons and positrons with energy above the critical energy of a material (typically tens of MeV), where their energy loss is completely dominated by bremsstrahlung radiation. At lower energies, electrons and positrons can inelastically interact through Coulomb collisions with atomic electrons to lose energy [38]. This leads to ionization and excitation, similar to the behavior observed in heavier particles. At even lower energies, in the MeV scale, electrons (positrons) also exhibit *Møller* (*Bhabha*) scattering.

3.4 Low energy gamma rays

Gamma-rays interact slightly differently from the charged particles due to their lack of electric charge. The three main interactions of gamma rays (and X-rays) are shown in Fig. 3.3.

An atomic electron can fully absorb the energy of a gamma ray[2], resulting in an electron with the energy of the initial gamma ray (MeV-scale) minus the binding energy of the atomic electron (eV-scale). This process is known as the *photoelectric effect*. As shown in Fig. 3.4, the photoelectric effect dominates for low-energy gamma-rays with a moderate-to-high density absorber.

[2]In order to conserve momentum, the photoelectric effect cannot occur on a free electron; it requires a nucleus to absorb part of the recoil.

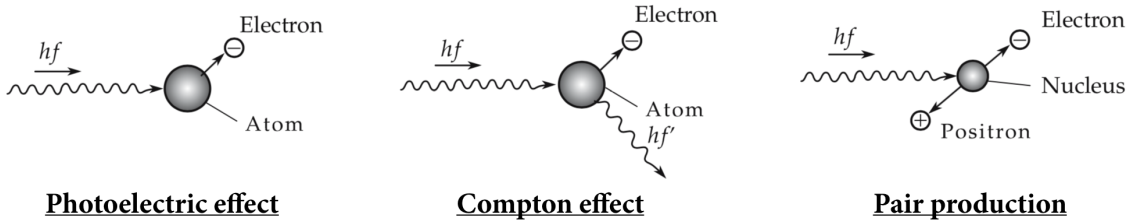

Figure 3.3: Modified from Ref. [32]

Compton scattering involves the partial transfer of energy from the incident gamma-ray to an atomic electron, leading to the electron's elevation to a higher energy level or ionization. The gamma-ray may alter its direction, exiting the material containing the electron, or it might undergo further scattering with another electron. Compton scattering prevails at low energy for materials with very low atomic numbers (Z), and the likelihood of scattering is directly proportional to the electron density, and thus, to the proton number of the material.

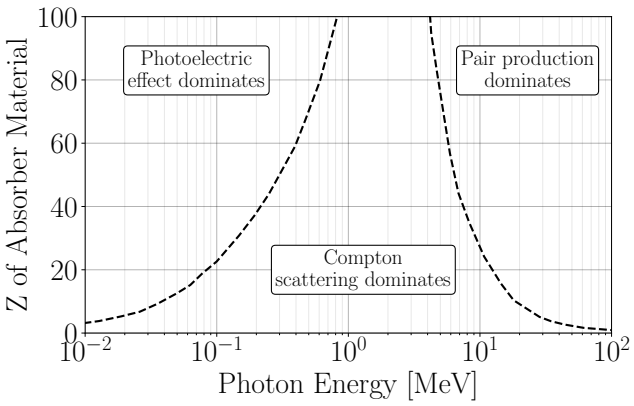

Figure 3.4: Dominant region for the three gamma ray interactions as a function of the photon energy and the target charge number Z. Modified from Ref. [8]

At energies above 1.022 MeV, electron-positron pair production plays a role. Pair production follows the same description as that found in the discussion of high-energy electrons (Sec. 3.2). The only difference is that the chain begins with a photon rather than an electron.

In addition, there are second-order effects, such as *Rayleigh scattering*, where the photon wavelength is large enough that it coherently scatters off the entire atom, and photonuclear interactions at higher energies that break up the nucleus [35].

3.5 Neutrons

Similar to photons, neutrons are not electrically charged, and thus, they do not undergo Coulomb interactions with electrons and nuclei. Instead, they interact through the strong force with nuclei. Due to the short-range nature of the strong force, these interactions are comparatively rare, as the neutron needs to approach the nucleus closely to interact. Several possible interactions are [7]:

1. Elastic scattering off a nucleus
2. Inelastic scattering off a nucleus, leaving the nucleus in an excited state that may decay by emitting a gamma ray. To excite the nucleus, the neutron must transfer MeV-scale energies.
3. Neutron capture. At low energies, the neutron might be captured by the nucleus, emitting a gamma ray.
4. Fission
5. Hadronic shower, particularly at high energies (> 100 MeV).

High-energy neutrons produced in the primary cosmic-ray interaction will often collide with another nucleus, creating a similar interaction as the primary cosmic-ray.

Chapter 4

Detection methods

4.1 Single Photon Detection: Photomultipliers

Photomultipliers stand as one of the prevalent tools in the toolkit of particle physicists. These devices possess the capability to generate a measurable electrical signal triggered by the interaction of a single photon. The detection of photons allows us to extract information about incident particles by observing the photon emission as the particle loses energy within a material.

A widely utilized instrument for single photon sensing is the photomultiplier tube (PMT), known for its expansive photosensitive coverage at a reasonable cost. Despite its effectiveness, PMTs come with the downside of being bulky, fragile, and requiring high voltage. Other technologies, such as Avalanche Photodiodes (APD) and P-type and N-type semiconductor photodiodes (PIN photodiode), present their own set of advantages and limitations.

Recent advancements in silicon chip manufacturing have given rise to a new breed of photon detectors known as *silicon photomultipliers*, or SiPMs (also abbreviated as SPM). SiPMs bring several advantages over PMTs, including the ability to operate at low voltages (we'll use +30.0V), insensitivity to magnetic fields, robustness, and a compact form factor. Serving as single photon detectors, SiPMs exhibit peak responsivity near the emission peak of typical scintillating materials (420 nm). This modern technology is the foundation of the Desktop Muon Detectors.

SiPMs are composed of densely arranged *microcells* (see Fig. 4.1), where each microcell constitutes a distinct P-type and N-type semiconductor junction (P-N junction). During the formation of a P-N junction, free electrons from the N-type semiconductor diffuse towards the P-type semiconductor, and vice versa, leading to their annihilation. This process establishes an insulating region known as the *depletion region* at the boundary between the P and N-type semiconductors.

As a photon travels through the depletion region and imparts sufficient energy to a bound electron, the electron can transition to the conduction band, generating an electron-hole pair. Applying a potential difference across the P-N junction enables the energized electron to collide with other electrons, initiating their transport into the conduction band. If the potential difference exceeds a critical value ($> 5 \times 10^5$ V/cm), an electron avalanche or cascade (resembling a Geiger discharge) occurs, wherein a single electron gives rise to a current comprising millions of electrons. Once the flow of electrons begins, the silicon becomes conductive, and a quenching resistor reduces the potential difference across the P-N junction sufficiently to halt the electron cascade. Consequently, each microcell functions as a photon-triggered switch, allowing a brief flow of a small current if struck by a photon. The cumulative current flow is proportional to the number of triggered microcells and, hence, is proportionate to the incident photon flux (when the number of triggering photons far exceeds the number of microcells).

The Desktop Muon Detector utilizes a single OnSemiconductor MicroFC 60035 C-Series SiPM, measuring 7.0 mm by 7.0 mm [39] (6 mm by 6 mm sensitive area). These SiPMs are most sensitive in the 420 nm range [40], corresponding to deep blue to purple light. I note that if the wavelength of a photon exceeds 1000 nm, the absorption length in silicon becomes too large, leading to the SiPM's size becoming impractical. On the other hand, if the photon wavelength is too short, it won't penetrate into the sensitive region of the SiPM, essential for effective detection.

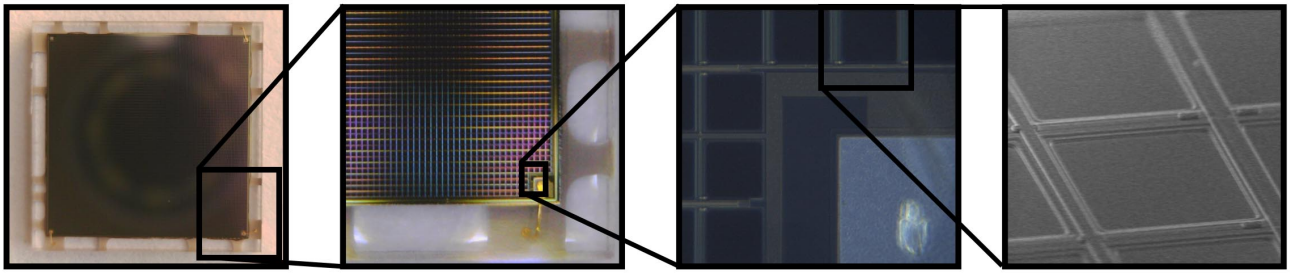

Figure 4.1: An image of an OnSemiconductor SiPM [39]. Data sheets found in the datasheet folder. The SiPM has a length and width of 7.0±0.05 mm and a thickness of 0.65±0.05 mm. Each one of the tiled squares represents a single microcell, each of which operate independently in Geiger mode.

The applied potential difference is referred to as the "bias voltage," and it determines both the size of the region capable of producing the avalanche (the depletion region) and the energy gained by the electron-hole pair. The "breakdown voltage" signifies the voltage at which the voltage gradient in the depletion region is sufficiently large to initiate a Geiger discharge. For the C-series SiPMs, this typically falls between 24.2 and 24.7 V. If the bias voltage surpasses the breakdown voltage, the microcells will still operate in Geiger mode; however, the electron cascade in the P-N junction will carry more energy, resulting in a linear increase in the charge output (or gain). The disparity between the bias voltage and the breakdown voltage is termed *over-voltage*. It is recommended to maintain an over-voltage between 1.0 and 5.0 V. The Desktop Muon Detectors operate with an over-voltage of roughly 6.0 V, corresponding to a gain of approximately 6×10^6 [39]. At this bias voltage, the photon detection efficiency at 420 nm is

roughly 43%.

Thermal fluctuations have the capability to generate electron-hole pairs, mimicking single photon events. For our SiPMs, this phenomenon occurs at a rate of approximately 100 kHz per mm^2, or several MHz for the entire SiPM! This can pose challenges for applications relying on the distinction between small numbers of photons. It's noteworthy that the breakdown voltage needed to initiate the electron cascade is temperature-dependent; lower temperatures correspond to lower breakdown voltages (21.5 mV/C°). For every 8°C decrease in temperature, the dark rate decreases by a factor of two. Gain is also impacted by the temperature. For very degree C change, the gain decreases by approximately 0.8%.

4.2 Scintillators

Scintillators are materials designed to absorb energy through Coulomb interactions and subsequently re-emit that energy in the form of electromagnetic radiation, known as scintillation light. Scintillators can take various forms; for instance, they may be grown as crystals (referred to as inorganic scintillators) with added dopants, or they might consist of a fluorescing material embedded in plastic materials such as polystyrene or acrylic, or mixed into liquids like toluene or mineral oil—examples of organic scintillators.

Inorganic scintillators are typically more expensive, but they often have higher density and emit more photons per unit energy deposited. This characteristic makes them particularly useful for calorimetry. On the other hand, organic scintillators are generally more affordable since the fluorescent material is suspended in a common, often low-density material like plastic, facilitating ease of manufacturing.

Scintillators are highly valuable materials as they emit light in proportion to the energy deposited in the material. Consequently, a common metric used to assess the quality of a scintillator is expressed as the number of photons emitted per absorbed MeV of energy, often referred to as the scintillator efficiency. For instance, a typical organic scintillator may exhibit an efficiency (light-yield) of 10,000 photons/MeV. Another crucial parameter associated with scintillators is the photon emission profile, determining the wavelengths of emitted photons after de-excitation. Moreover, scintillators must be transparent to scintillation light to enable its propagation to the photon detector. Plastic scintillators may have attenuation lengths ranging from 0.3 meters to 3 meters [41, 42], while liquid scintillators like Linear Alkyl Benzene (LAB) can have attenuation lengths of up to 25 meters [43]. Scintillators also exhibit a very fast response and recovery, with excitation and de-excitation of the fluorescing molecules occurring on the order of nanoseconds for organic scintillators and hundreds of nanoseconds for inorganic scintillators.

The CosmicWatch Desktop Muon Detector was designed using an organic plastic scintillator, comprising a polystyrene base (essentially an inexpensive transparent plastic) mixed with a primary dopant of 1% by weight of POP (2,5-diphenyloxazole) and 0.03% secondary dopant

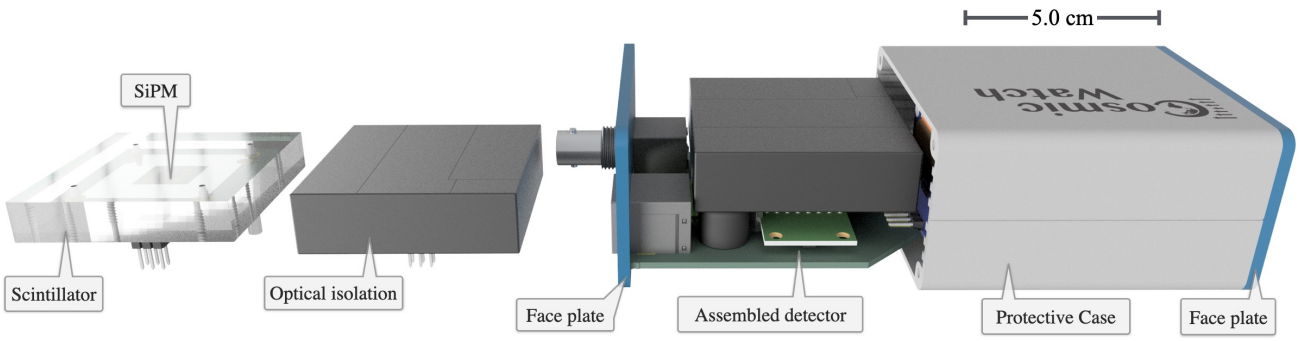

Figure 4.3: The components of the Desktop Muon Detector.

POPOP (1,4-bis[2-(5-phenyloxazolyl)]benzene) [44][1]. This plastic scintillator does not emit light below 400 nm and has a maximum emission around 420 nm (deep-purple light). Developed by FermiLab for the MiNOS [46]/MINERνA [47] experiments, we will focus on a description of organic scintillators below. However, a comprehensive description of inorganic scintillators can be found in Ref. [45].

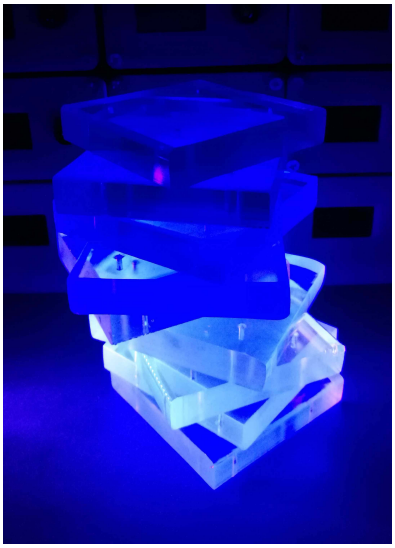

Figure 4.2: A UV flash light illuminating scintillator.

The plastic scintillator consists of three essential components:

- A transparent base, visible in the visible spectrum, used to suspend the fluorescent material. This can be a type of plastic (such as polystyrene) or a transparent liquid like mineral oil.
- A primary fluorescing agent excited by the energy transfer from the incident charged particle. The de-excitation of the primary fluorescent material releases ultraviolet (UV) light. UV light has a limited travel distance in the base (on the order of millimeters) before being absorbed.
- A secondary fluorescent agent that absorbs the UV light and converts it to the visible spectrum. The visible light then travels through the scintillator, internally reflecting off the walls until it is absorbed. Ideally, some of the visible light will strike the photon sensor coupled to the scintillator.

A straightforward representation of the UV conversion process is depicted in Fig. 4.2. In this illustration, several pieces of scintillator are illuminated with a UV flashlight. The UV light is absorbed by the secondary fluorescent agent and re-emitted as deep blue/purple light. A polystyrene-based scintillator typically has a density of approximately 1.032 g/cm^3 (similar to water) and

[1]Interestingly, PPO was one of the earliest compounds investigated as a scintillator solute by Hayes et al. (see Ref. [45]) from 1953-1958 and is still widely used

a refractive index at standard atmospheric pressure of $n = 1.581$ [8]. Recall, from your optics class, that air has a refractive index of $n = 1.00$.

The Desktop Muon Detector couples a SiPM (see Sec. 4.1) to a slab of scintillator through optical gel (and/or thin silicone pad), which reduces the probability of a photon being reflected at the interface by matching the refractive index from the scintillator to the housing of the SiPM, eliminating the air gap. Additionally, the remaining surface is wrapped in aluminum foil to reflect photons that escape the scintillator. The entire assembly is then covered with 2-3 layers of black electrical tape to ensure light-tightness. The assembly of the detector is illustrated in Fig. 4.3.

Chapter 5

Additional things you should know

5.1 Accidental coincident events

: Two distinct events (like two independent gamma rays) might accidentally trigger both detectors setup in coincidence mode if they happen to occur within the coincidence time window τ. This is referred to as an accidental coincidence. This probability increases at higher count rates. Assuming that individual count rates follow Poisson statistics and that the events are independent, the probability of observing n events when the mean number of events expected is μ, is described by the Poisson distribution:

$$f(n, \mu) = \frac{\mu^n e^{-\mu}}{n!} \tag{5.1}$$

Let's assume you turned on both detectors and measured the individual master count rates: N_1 and N_2. We will now calculate the rate at which two events happen to occur within a time window τ.

The probability that Detector 2 gives no signal in the time interval τ is:

$$f(0, N_2\tau) = e^{-N_2\tau} \tag{5.2}$$

Correspondingly, the chance of getting an uncorrelated count in this window is 1 - f(0,$N_2\tau$):

$$P = 1 - e^{-N_2\tau} \tag{5.3}$$

Since normally $N_2\tau \ll 1$, we can Taylor expand:

$$P \simeq -N_2\tau \tag{5.4}$$

This is the probability of Detector 2 observing a count in time window τ. The rate of which the time window τ is opened is N_1 (Detector 1 trigger rate). Therefore, the rate at which Detector 2 observes a count in coincidence with Detector 1 is:

$$R_2 = N_1 N_2 \tau \tag{5.5}$$

Finally, Detector 2 can also have a signal before Detector 1 within the resolving time of the coincidence circuit, **the total accidental coincidence rate is**:

$$R_{acc} = 2N_1 N_2 \tau \tag{5.6}$$

For example: the average count rate for both detectors at sea level is approximately 3 Hz, and given a coincident time window of roughly 3μs, we expect the mean number of events in the time window to be $9{\times}10^{-9}$ ($N_{1,2} \times \tau$). Therefore, the probability of observing zero events in the time window is $f(0, 9 \times 10^{-6})$, and the probability of one detector observing an event in the coincident time window is $1 - f(0, 9 \times 10^{-6})$. Since the second detector could have also triggered first, the rate of accidental triggers is given by: $R_acc = 2N_1 N_2 \tau$ (Eq. 5.1). This corresponds to an accidental coincident rate of 54 μHz for two detectors, or equivalently of 1 every 55,555 events, or roughly one to two events per day using two detectors, at sea level with common background levels.

But, what happens at 60,000 feet, when both detectors trigger at 60 Hz? The accidental rate is 0.02 Hz! Much higher.

5.2 Are coincidence events pure muons?

Electromagnetic contribution from the shower

Looking at Fig. 2.2, you might wonder what other particles are able to trigger the detectors. Well, at sea level, I would argue that there is a population of low energy (sub-GeV) electrons that cascade down and are capable of triggering two detectors in coincidence. In fact, outside, in open air, with no overburden (overhead shielding), this is approximately 0.1 Hz, or around 30% of the coincidence rate. The good news is that you can simply move under some concrete to shield the detectors from this component of the flux. If you want to make a "pure" muon measurement, make sure to go under a foot of concrete of more to get rid of this low energy electromagnetic component of the flux.

Proton contribution from the shower

: At sea level, maybe 1 in a 100 recorded coincident events will actually be a proton. You can't really get rid of these in an efficient way. However, more importantly, is that if you take these detectors to high altitudes, the composition of the flux dramatically changes. At about 5 km, muons are no longer the dominant source of charged particles particles that can trigger a pair of coincidence detectors. In fact, it's protons. So, even though we call these muon detectors, at high altitudes, like the airplane and high altitude balloon measurements shown in the Example Measurements Document, those are primarily proton measurements.

5.3 The muons are coming straight downwards, no?

No. The maximum flux per unit area on the sky is vertical downwards, however, there's way more area as that angle moves away from the zenith. If you take the cosmic ray muon angular distribution to follow a cosine squared dependence, and convolve with the relative area of a band in the sky, you would find that the largest number of muons is actually comming in around 35 degrees below the zenith.

5.4 What is dead time?

The RPi is an inexpensive (4 USD) and relatively slow device compared to other much more expensive devices. While being a fairly new MCUs, inherent issues arise due to its speed limitations. An important aspect of any rate measurement with any detector is that every command, whether it involves simple arithmetic or printing detector information to the serial port or microSD card, takes time to execute. If during that time, the detector cannot monitor for incoming signals (i.e. it is dead), you need to account for that time. The term associated with the time during which the detector is unable to make a measurement is referred to as *dead time*. The detector software code calculates the dead time by measuring how long each command (or sets of commands) takes. The cumulative dead time up to the event you are looking at is recorded in the data output. To obtain an accurate measurement of the time the detector was able to make a measurement, the dead time must be subtracted from the total runtime; the result is termed *livetime*. dead time is a common feature in nearly all particle physics detectors. It becomes more problematic as rates increase as well, as part of the dead time might be associated with creating and reading out the event. At sea level, the dead time may affect the rate by 0.5%, while in a high-altitude balloon at 60,000 feet, where the count rates approach 60 Hz, the dead time impacts the rate measurement by roughly 3%. We strategically use dual cores with specially data buffering techniques to reduce the dead time as much as possible. For context, the dead time per event is more than two orders of magnitude lower than the previous published version of the detector.

Chapter 6

Conclusion

The CosmicWatch Desktop Muon Detectors offer a versatile platform for exploring diverse natural phenomena. This document provided a comprehensive overview of the underlying physical processes influencing the detectors and demonstrated how valuable insights can be derived from the collected data. The detectors can be employed to investigate a wide range of phenomena related to the geomagnetic field, atmospheric conditions, cosmic-ray shower composition, particle attenuation in matter, radioactivity, and statistical properties of Poisson processes. Students are encouraged to further develop the concepts introduced or design their experiments. Feedback is highly welcomed to enhance and refine this manual. Enjoy your exploration with the CosmicWatch detectors!

Bibliography

[1] K. O. et al, "Cosmic rays - particle data group," *Nuclear Instruments and Methods in Physics Research Section A: Accelerators, Spectrometers, Detectors and Associated Equipment*, vol. 38, no. 090001, p. 6, 2014.

[2] S. K. LBNL, *32. PASSAGE OF PARTICLES THROUGH MATTER*. LBNL, 2017.

[3] B. Rossi, *Cosmic Rays*. New York: McGraw-Hill, 1964.

[4] M. W. Friedlander, *A thin cosmic rain: Particles from outer space*. Harvard University Press, 2002.

[5] P. K. Grieder, *Cosmic rays at Earth*. Elsevier, 2001.

[6] T. K. Gaisser, R. Engel, and E. Resconi, *Cosmic rays and particle physics*. Cambridge University Press, 2016.

[7] W. R. Leo, *Techniques for nuclear and particle physics experiments: a how-to approach*. Springer Science & Business Media, 2012.

[8] C. Grupen and B. Shwartz, *Particle detectors*, vol. 26. Cambridge university press, 2008.

[9] H. Kolanoski and N. Wermes, *Particle detectors: fundamentals and applications*. Oxford University Press, 2020.

[10] D. Bird, S. Corbató, H. Dai, B. Dawson, J. Elbert, T. Gaisser, K. Green, M. Huang, D. Kieda, S. Ko, *et al.*, "Evidence for correlated changes in the spectrum and composition of cosmic rays at extremely high energies," *Physical review letters*, vol. 71, no. 21, p. 3401, 1993.

[11] G. Taubes, "Pattern emerges in cosmic ray mystery," *Science*, vol. 262, no. 5140, pp. 1649–1650, 1993.

[12] F. Halzen and A. D. Martin, "Quarks and leptons," 1984.

[13] D. Griffiths, *Introduction to elementary particles*. John Wiley & Sons, 2008.

[14] M. Fukugita and T. Yanagida, *Physics of Neutrinos: and Application to Astrophysics*. Springer Science & Business Media, 2013.

[15] M. Tanabashi, P. Richardson, A. Bettini, A. Vogt, L. Garren, A. J. Schwartz, K. Terashi, M. Karliner, R. S. Chivukula, T. Sjöstrand, *et al.*, "Aps: Review of particle physics," *Phys. Rev. D*, vol. 98, p. 030001, 2018.

[16] T. K. Gaisser and M. Honda, "Flux of atmospheric neutrinos," *Annual Review of Nuclear and Particle Science*, vol. 52, no. 1, pp. 153–199, 2002.

[17] E. Regener and G. Pfotzer, "Vertical intensity of cosmic rays by threefold coincidences in the stratosphere," *Nature*, vol. 136, no. 3444, p. 718, 1935.

[18] O. Allkofer, R. Andresen, and W. Dau, "The muon spectra near the geomagnetic equator," *Canadian Journal of Physics*, vol. 46, no. 10, pp. S301–S305, 1968.

[19] O. Allkofer, R. Andresen, K. Clausen, and W. Dau, "Sea-level muon spectrum at two different latitudes," *Journal of Geophysical Research*, vol. 77, no. 22, pp. 4251–4253, 1972.

[20] C. Augusto, C. Navia, and K. Tsui, "Muon enhancements at sea level in association with swift-bat and milagro triggers," *Physical Review D*, vol. 77, no. 12, p. 123008, 2008.

[21] https://www.nasa.gov/mission_pages/station/research/experiments/1043.html, "International space station internal radiation monitoring (iss internal radiation monitoring) - 04.05.17," Dec 2018.

[22] T. Dachev, W. Atwell, E. Semones, B. Tomov, and B. Reddell, "Observations of the saa radiation distribution by liulin-e094 instrument on iss," *Advances in Space Research*, vol. 37, no. 9, pp. 1672–1677, 2006.

[23] L. Pinsky, W. Osborne, J. Bailey, R. Benson, and L. Thompson, "Light flashes observed by astronauts on apollo 11 through apollo 17," *Science*, vol. 183, no. 4128, pp. 957–959, 1974.

[24] C. Fuglesang, L. Narici, P. Picozza, and W. G. Sannita, "Phosphenes in low earth orbit: survey responses from 59 astronauts," *Aviation, space, and environmental medicine*, vol. 77, no. 4, pp. 449–452, 2006.

[25] A. Rinaldi, "Phosphenes in space: a study on the interaction between carbon ions and rod photoreceptor," 2009.

[26] C. Augusto, C. Navia, H. Shigueoka, K. Tsui, and A. Fauth, "Muon excess at sea level from solar flares in association with the fermi gbm spacecraft detector," *Physical Review D*, vol. 84, no. 4, p. 042002, 2011.

[27] M. Savić, D. Maletić, D. Joković, N. Veselinović, R. Banjanac, V. Udovičić, and A. Dragić, "Pressure and temperature effect corrections of atmospheric muon data in the belgrade cosmic-ray station," in *Journal of Physics: Conference Series*, vol. 632, p. 012059, IOP Publishing, 2015.

[28] P. H. Barrett, L. M. Bollinger, G. Cocconi, Y. Eisenberg, and K. Greisen, "Interpretation of cosmic-ray measurements far underground," *Reviews of Modern Physics*, vol. 24, no. 3, p. 133, 1952.

[29] F. An, A. Balantekin, H. Band, M. Bishai, S. Blyth, D. Cao, G. Cao, J. Cao, Y. Chan, J. Chang, *et al.*, "Seasonal variation of the underground cosmic muon flux observed at daya bay," *Journal of Cosmology and Astroparticle Physics*, vol. 2018, no. 01, p. 001, 2018.

[30] A. Bouchta, "Seasonal variation of the muon flux seen by amanda," in *International Cosmic Ray Conference*, vol. 2, p. 108, 1999.

[31] M. Ambrosio, R. Antolini, G. Auriemma, R. Baker, A. Baldini, G. Barbarino, B. Barish, G. Battistoni, R. Bellotti, C. Bemporad, *et al.*, "Seasonal variations in the underground muon intensity as seen by macro," *Astroparticle Physics*, vol. 7, no. 1-2, pp. 109–124, 1997.

[32] W. Benenson, J. W. Harris, H. Stöcker, and H. Lutz, *Handbook of physics*. Springer Science & Business Media, 2006.

[33] D. Green, *The physics of particle detectors*, vol. 12. Cambridge University Press, 2000.

[34] W. Li, M. D. Rodriguez, P. Kluth, M. Lang, N. Medvedev, M. Sorokin, J. Zhang, B. Afra, M. Bender, D. Severin, *et al.*, "Nu clear instrum ents and methods in phy sics research b," *Nuclear Instruments and Methods in Physics Research B*, vol. 302, pp. 40–47, 2013.

[35] K. A. Olive *et al.*, "Review of Particle Physics," *Chin. Phys.*, vol. C38, p. 090001, 2014.

[36] B. R. Martin, *Nuclear and particle physics: an introduction*. John Wiley & Sons, 2006.

[37] T. Tabata, R. Ito, and S. Okabe, "An empirical equation for the backscattering coefficient of electrons," *Nuclear instruments and methods*, vol. 94, no. 3, pp. 509–513, 1971.

[38] M. J. Berger and S. M. Seltzer, "Stopping powers and ranges of electrons and positions," tech. rep., NATIONAL STANDARD REFERENCE DATA SYSTEM, 1982.

[39] https://www.onsemi.com/pub/Collateral/AND9770 D.PDF, "On semiconductor: Introduction to the silicon photomultiplier," Dec 2018.

[40] https://www.sensl.com/downloads/ds/TN

[41] A. Pla-Dalmau, A. D. Bross, V. V. Rykalin, and B. M. Wood, "Extruded plastic scintillator for minerva," in *Nuclear Science Symposium Conference Record, 2005 IEEE*, vol. 3, pp. 1298–1300, IEEE, 2005.

[42] Eljen. https://eljentechnology.com/products/plastic-scintillators, accessed: Oct 2018 2018.

[43] H. Yang, D. Cao, Z. Qian, X. Zhu, C. Loh, A. Huang, R. Zhang, Y. Yang, Y. Liu, B. Xu, *et al.*, "Light attenuation length of high quality linear alkyl benzene as liquid scintillator solvent for the juno experiment," *Journal of Instrumentation*, vol. 12, no. 11, p. T11004, 2017.

[44] D. Beznosko, A. Bross, A. Dyshkant, and P.-D. Rykalin, "Fnal-nicadd extruded scintillator," in *Nuclear Science Symposium Conference Record, 2004 IEEE*, vol. 2, pp. 790–793, IEEE, 2004.

[45] D. Horrocks, *Applications of liquid scintillation counting*. Elsevier, 2012.

[46] I. Ambats, Y. Antipov, A. Sadovski, K. Lang, W. Allison, D. Wall, A. Napier, Y. Lai, R. Heinz, D. Wright, *et al.*, "The minos detectors technical design report," tech. rep., FNAL, 1998.

[47] L. Aliaga, L. Bagby, B. Baldin, A. Baumbaugh, A. Bodek, R. Bradford, W. Brooks, D. Boehnlein, S. Boyd, H. Budd, *et al.*, "Design, calibration, and performance of the minerva detector," *Nuclear Instruments and Methods in Physics Research Section A: Accelerators, Spectrometers, Detectors and Associated Equipment*, vol. 743, pp. 130–159, 2014.